Composites Science and Technology 204 (2021) 108605

Contents lists available at ScienceDirect

Composites Science and Technology

journal homepage: http://www.elsevier.com/locate/compscitech

Enhanced mode II fracture toughness of secondary bonded joints using tailored sacrificial cracks inside the adhesive

A. Wagih, G. Lubineau *

King Abdullah University of Science and Technology (KAUST), Physical Science and Engineering Division, COHMAS Laboratory, Thuwal, 23955-6900, Saudi Arabia

ARTICLE INFO

Keywords:
Adhesive joints
Fracture toughness
Damage mechanics
Non-destructive testing
Tailored sacrificial cracks

ABSTRACT

The mode II fracture toughness of secondary bonded joints can be improved by creating tailored sacrificial cracks inside the adhesive. To this end, we inserted a PTFE film inside the adhesive bondline during the bonding process to create sacrificial cracks inside the adhesive. We demonstrated the efficiency of this technique through ENF tests that characterize mode II fracture toughness of adhesive-bonded CFRP adherends. We ascribed the improvement in toughness to the reduction of the strain concentration at the crack tip, which delayed the crack propagation and thus improved joint initiation fracture toughness, G_{IIi}, and the maximum load capacity, P_{max}. Moreover, after crack propagation, sacrificial cracks arrested the crack propagation at the upper interface, grew secondary backward cracks at the lower interface, and created adhesive ligaments. These three damage mechanisms dissipated more energy during propagation, which improved the propagation fracture toughness, G_{IIc}. The improvement rates depend on the sacrificial crack width and the gap between two successive cracks reaching 96%, 98%, and 25% for G_{IIi}, G_{IIc} and P_{max}, respectively, for a 2 mm sacrificial crack width and 5 mm gap. Our approach works well for both thin and thick adhesives and is a simple technique to substantially enhance the toughness of secondary bonded joints.

1. Introduction

Most composite structures are made by combining smaller parts that are manufactured separately. Mechanical fastening, and adhesive bonding are the most common methods. Traditional fasteners usually require drilling holes in the structure and different machining processes, which may cause initial internal damage in the composite part, such as matrix cracks and delaminations. Moreover, cutting the fibers causes a decrease in the load carrying capacity of the part, which requires extra material, and thus increases the structure weight [1]. Bonded joints are increasing popular alternatives to mechanical joints in engineering applications due to their advantages over conventional mechanical fasteners. Among these advantages are lower stress concentrations, increased strength-to-weight efficiency, and improved damage tolerance [2]. The application of these joints in structural components made of fiber reinforced composites has increased significantly in recent years. However, the catastrophic failure of these joints limits their application as a primary joining technique for structural applications. These adhesive joints usually fail in an unstable manner once a crack is initiated because the crack can propagate very rapidly, thus causing catastrophic failure. To this end, efforts have been made in the literature to arrest crack propagation, not only by improving the adhesive-adherend interface toughness but also by improving the R-curve response of these joints, and ultimately avoid catastrophic failure can be avoided.

Several techniques are presented in the literature to improve fracture toughness of bonded joints. We can categorize these techniques as adherend-based modifications and adhesive-based modifications. The adherend-based modifications mainly increase the surface roughness of the adherend using methods such as sanding, grit blasting, and peel-ply [3–5], which allows better adhesion at the interface and thus improves interface toughness. Despite the effectiveness of sanding and grit blasting to produce relatively rough surfaces, the joints are still not reliable because both methods are manually operated, which introduces a large variation in the joint strength and toughness. Moreover, these techniques can cause fiber damage at the interface, which reduces the adherend strength [6]. Peel-ply is applied to overcome the disadvantages of these techniques; however, its applicability for large structures is limited because it must be applied before adherend curing [4]. Recently, UV, CO_2 and femtosecond laser treatment [7–9] have been applied to increase adherend surface roughness. A previous study

* Corresponding author.
E-mail addresses: ahmed.abdelhady.1@kaust.edu.sa (A. Wagih), gilles.lubineau@kaust.edu.sa (G. Lubineau).

https://doi.org/10.1016/j.compscitech.2020.108605
Received 5 July 2020; Received in revised form 16 November 2020; Accepted 3 December 2020
Available online 13 December 2020

proposed [10] the application of CO_2 laser treatment with alternating high and low energy for both adherends to produce two different surface roughness, which activates nonlocal damage mechanisms. These damage mechanisms dissipate higher energy during propagation, thereby improving the fracture toughness. Additionally, the same treatment strategy has been applied to improve Mode I fracture toughness [11,12].

On the other hand, adhesive-based modification has been proposed in several studies, including z-pinning and stitching [13–16], ceramic additives [17,18] and thermoplastic inclusions [19–21]. However, although z-pinning and stitching improve the fracture toughness of a bonded joint, the in-plane strength and stiffness are severely reduced due to fiber waviness [13].

Another approach consists in tailoring the microstructure of the composite to improve a particular property. This method is sometimes applied for composites to improve their fracture toughness. For example, Chudnovsky and Wu [22], reported improved fracture toughness with a large array of microcracks parallel to the main crack. The toughness improvement was due to the dissipation of energy in these microcracks and their elastic deformation. Recently, Bullegas et al. [23] applied the same philosophy to improve translaminar fracture toughness of thin-ply laminates. They achieved a 3-fold improvement in fracture toughness by generating microcracks with certain patterns along the crack path. Maloney and Fleck [24] embedded woven copper mesh inside the adhesive of a metallic bonded joint with sequential insertion of defects on alternating surfaces of adherends to improve the fracture toughness of bonded joints.

Inspired by this philosophy, here we propose the generation of tailored sacrificial cracks inside the adhesive bondline to improve mode II fracture toughness of secondary bonded joints. We use a PTFE film with a designed width to generate these sacrificial cracks during the bonding process. We study the effect of sacrificial crack width and the effect of the gap between two successive cracks to understand the mechanisms that leads to improved fracture toughness. We perform an ENF test and apply an effective crack length data reduction method to characterize mode II fracture toughness. We employ a digital camera to capture real time photos of the sample edges during the test and X-Ray micro-computed tomography (μ-CT) to identify the internal damage mechanisms. We analyze thin and thick adhesives with thicknesses of 0.3 and 0.8 mm to identify the applicability range of our proposed technique. Thus, the paper is organized as follows: in the next section, we describe in detail the bonding process followed to generate sacrificial cracks inside the adhesive, the tests that we carry out and the data reduction method that we use. Then, in the third section, we present the experimental results obtained during the test. Finally, we discuss the results to highlight the toughening mechanisms of bonded joints with sacrificial cracks, the topology effect of these cracks, and the adhesive thickness effects.

2. Experiments and methods

2.1. Specimen preparation

We used unidirectional tape prepreg carbon/epoxy (T700/M21 Hexply, Hexcel) to manufacture the adherends of secondary bonded joints. We used the hand lay-up technique to stack eight plies of 0.25 mm thickness to produce adherends with $[0^\circ]_8$ stacking sequence and 2 mm thickness. After laying up of the 300 × 300 mm^2 panels, we used compression molding to cure these plates. We compressed the samples at 7 bar pressure and 180 °C for 2 h using a hydraulic hot press that was programmed with constant heating and cooling rates of 3 °C/min. We followed the ASTM standard recommendations to characterize the elastic material properties of the manufactured adherends, which are summarized as: In-plane elastic modulus, $E_{11} = 135 \pm 6$ GPa; out-of-plane elastic modulus, $E_{22} = 8.75 \pm 0.27$ GPa; in-plane shear modulus, $G_{12} = 4.93 \pm 0.14$ GPa; in-plane Poisson's ratio $\nu_{12} = 0.29 \pm 0.01$.

We used an abrasive water jet machine to cut adherends from the manufactured panels. First, we trimmed 15 mm from the panel edges. Then, we cut the panels to 270 × 90 mm^2, i.e., three sub-panels. the major dimension was aligned with 0°.

Based on our previous work [10], we applied uniform laser treatment, using a CO_2 pulsed laser, to the adherend surface to improve adhesion between the adhesive and the adherend. The parameters used for laser treatment were: focal distance = 50 mm, Spot diameter = 200 μm, speed = 500 mm/s, pulse frequency = 20 kHz, and laser power = 22.5 W. After that, we submerged the sub-panels for 10 min in acetone, dried them at 60°C for 30 min and air-cleaned them.

We also used laser also to create rectangular cutouts in a non-adhesive Polytetrafluoroethylene film (PTFE) that acted as sacrificial cracks inside the adhesive layer. The uncut parts of the PTFE film (referred as *B* in Fig. 1 (a)) acted as cracks inside the adhesive layer since they have very low adhesion with adhesives, while the adhesive is continues through the cutouts (referred as *g* in Fig. 1(a)).

2.2. Adhesive bonding with tailored sacrificial cracks

We used Araldite 420 A/B adhesive (Elastic modulus = 1.5 GPa and Tensile strength = 36 MPa) to bond adherends after laser treatment. The bonding process was performed in three steps. First, we spread approximately half the thickness of the adhesive layer over one of the adherends. Then, we placed the PTFE film with cutouts over the first half of the adhesive layer. After that, we spread the other half of the adhesive over the second adherend and bonded them together. The bonding steps are shown in Fig. 1(a). After bonding, we placed the bonded sub-panels in a furnace at 60°C for 30 min under vacuum and at the same temperature for 3 h without vacuum followed by storing at room temperature for 24 h. Finally, we cut each bonded sub-panel into three samples of 260 mm × 25 mm, where the major dimension was aligned with the fiber direction.

2.3. ENF test and data reduction method

We used the ENF test (see Fig. 2) to characterize the Mode II fracture toughness of secondary bonded joints with tailored sacrificial cracks. We followed the ASTM D7905 standard for the sample size with slight modification on the ratio of half-span length (L) to initial crack length (a_0) to achieve stable crack propagation. Carlsson et al. [25] reported that a a_0/L ratio should be equal or larger than 0.7 to achieve stable crack propagation. However, in the current study, with this parameter at $a_0/L = 0.7$, the crack propagation was not stable. Following a review of more recent works, we noted that the value of a_0/L needed to achieve stable crack propagation can vary widely. For example, Hashemi et al. [26] studied different a_0/L ratios, 0.5–0.7, and demonstrated that all the considered values gave unstable crack propagation. Moreira et al. [7] achieved stable crack propagation with $a_0 = 80$ mm and L = 120, giving an $a_0/L = 0.67$. Budzik et al. [27] achieved stable crack propagation with $a_0 = 44$ mm and L = 90, giving an $a_0/L = 0.49$. More recently, Pérez-Galmés et al. [28] performed an ENF test for two different adhesive materials with $a_0 = 35$ mm and L = 60 mm, giving an $a_0/L = 0.58$. They achieved stable crack propagation when testing one kind of adhesive but unstable crack propagation for some sample of the other adhesive. Based on this review, we performed several trials to reach our own a_0/L that achieved stable crack propagation [10]. We designed our experiment with $a_0/L = 0.44$, which achieved stable crack propagation for all the considered configurations. We placed a steel wire with diameter equal to the adhesive thickness between the two adherends, 5 mm from the support at the free edge, to ensure non-contact between the adherend's ends [7,27]. We applied displacement under a displacement control regime with a 0.5 mm/mm strain rate, and used a digital camera to monitor the crack growth evolution from the sample edge. Moreover, we synchronized these in situ photos with the load displacement data to explore the relationship between different external damage morphologies and the load-displacement response. We designed

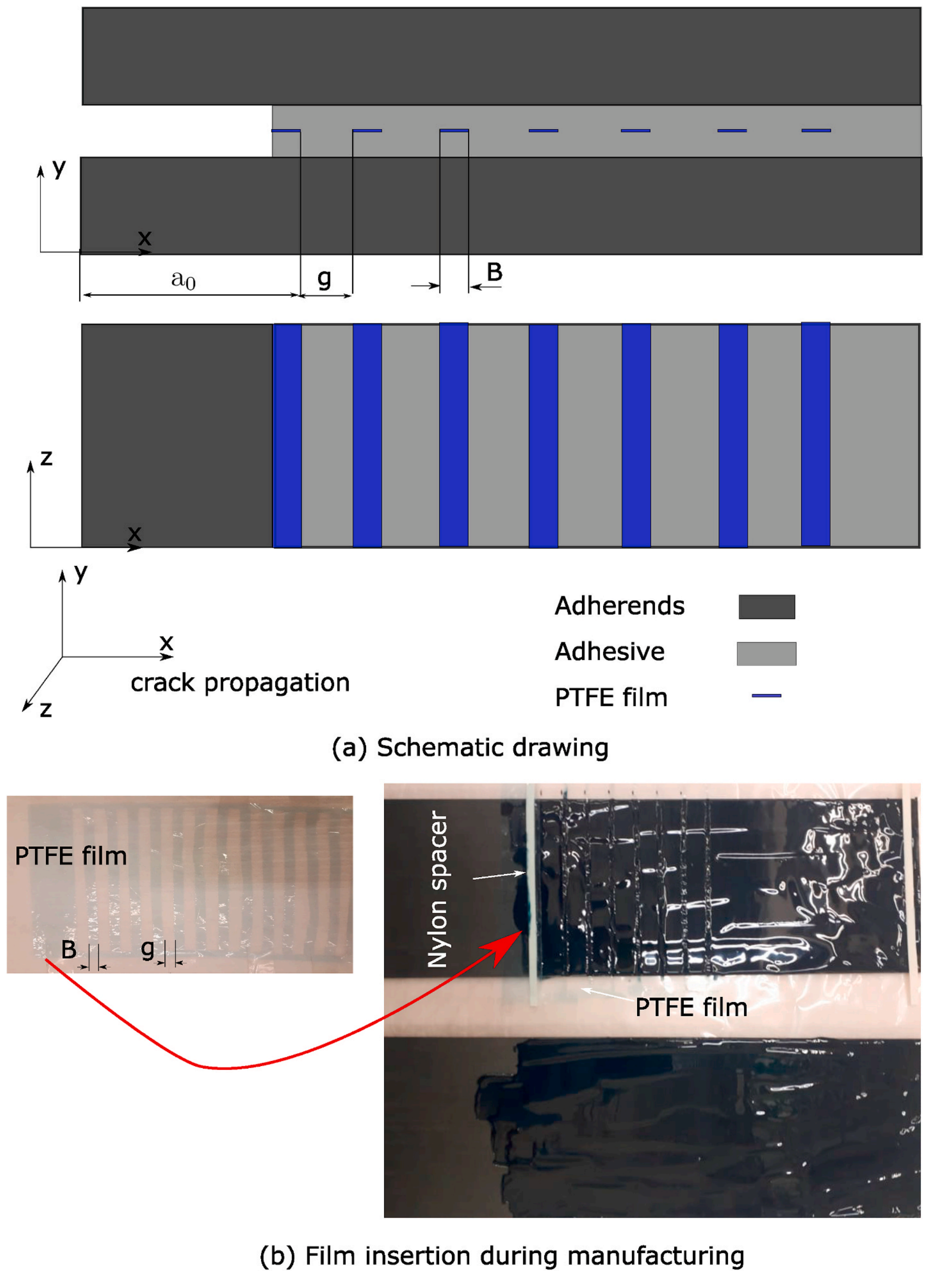

Fig. 1. Schematic drawing of secondary adhesive bonded joints with sacrificial cracks (a) and photos of the PTFE film insertion process (b).

our test matrix as shown in Table 1 to study the effect of sacrificial crack width, B, and the gap between two successive sacrificial cracks, g, and adhesive thickness, h_a.

We used the effective crack length-based data-reduction method to overcome the difficulties of monitoring crack growth during loading. In the ENF test, due to compressive stresses in the crack growth path, the crack tends to grow at the interface while its surfaces are in contact. Moreover, the thick adhesive, 0.8 mm in some cases, leads to large deformation in the Failure Process Zone (FPZ), which results in larger energy dissipation. Additionally, the high ductility of the adhesive contributes to the increasing FPZ, which also increases the energy dissipation. Therefore, the effective crack-length based data-reduction method is adequate in this case because it considers all these dissipation mechanisms. In this method, we used Timoshenko Beam Theory (TBT) to compute the specimen compliance under bending as [10,29]:

$$C = \frac{\delta}{P} = \frac{3a^3 + 2L^3}{8bh^3 E_f} + \frac{3L}{10G_{13}bh} \tag{1}$$

where G_{13} is the adherend flexural modulus and E_f is the equivalent flexural modulus. To calculate E_f, we substitute the initial crack length a_0 and initial compliance C_0, that were computed at the early stage of loading, in Eq. (1), which then leads to:

$$E_f = \frac{3a_0^3 + 2L^3}{8bh^3}\left(C_0 - \frac{3L}{10G_{13}bh}\right)^{-1} \tag{2}$$

where a_e was calculated using Eq. (1). By taking into account E_f, Eq. (1) can be written as a function of the specimen compliance as follows:

$$a_e = \left[\frac{C_c}{C_{0c}}a_0^3 + \frac{2}{3}\left(\frac{C_c}{C_{0c}} - 1\right)L^3\right]^{1/3} \tag{3}$$

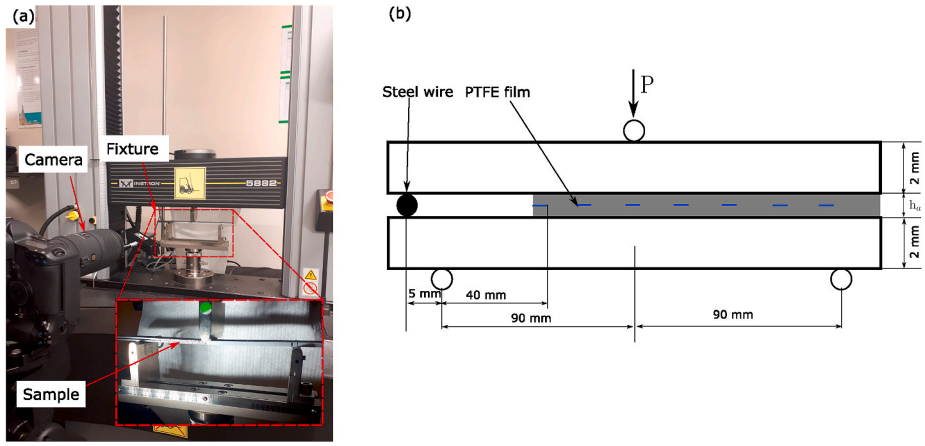

Fig. 2. Experimental test (a) setup and (b) schematic representation of ENF specimen and test geometry.

Table 1
Test matrix of sacrificial crack insertion.

Label	g, mm	B, mm	h_a, mm
BL-T008	0	0	0.8
G05B02-T008	5	2	0.8
G05B05-T008	5	5	0.8
G10B02-T008	10	2	0.8
G10B05-T008	10	5	0.8
G15B02-T008	15	2	0.8
G15B05-T008	15	5	0.8
BL-T003	0	0	0.3
G05B02-T003	5	2	0.3

where

$$C_c = C - \frac{3L}{10G_{13}bh}; C_{0c} = C_0 - \frac{3L}{10G_{13}bh} \tag{4}$$

According to linear elastic fracture mechanics, G_{II} can be computed as:

$$G_{II} = \frac{P^2}{2b}\frac{dC}{da} \tag{5}$$

Finally, by substituting Eq. (1) into Eq. (5), the direct relation between G_{II} and a_e can be approximated as:

$$G_{II} = \frac{9P^2a_e^2}{16b^2h^3E_f} \tag{6}$$

2.4. Postmortem analysis

We employed X-Ray micro-computed tomography (μ-CT) to identify the internal damage modes in some of the tested specimens. For better visualization of the damage and due to the fact that the two adherends were not completely separated after testing, we inserted a thick steel strip of 2 mm thickness between the adherends in the unbonded area. We used 60 kV voltage, 100 μA intensity, 250 ms exposure time, 11.27 μm voxel size, and a 26 mm field of view to gather 2500 projections of the specimen. We used CT Pro 3D to reconstruct the obtained projections.

2.5. Finite element simulation

We simulated the elastic response of the ENF test with sacrificial cracks using the ANSYS commercial FE software to observe strain state changes after embedding sacrificial cracks in the thin and thick adhesives. We used 2D plain strain elements to simulate the adherends and the adhesive layer. We defined the indenter as a rigid body with a pilot node, where the displacement was applied. We used a surface-to-surface contact algorithm to define contact between the indenter and the upper surface of the adherend. For the sake of simplicity and to avoid unnecessary contact surface, the contact between the lower adherend and the roller supports was substituted with an equivalent boundary condition by constraining x and y displacements of the node in the lower right corner and constraining the y displacement of the node in the lower left corner. The node in the lower left corner of the upper adhered was constrained in the y displacement to simulate the presence of the steel wire (see Fig. 3). We defined fully bonded interface between the adhesive and adherend, and employed the linear elastic material model to define both adherends and adhesive using the elastic properties previously reported in Section 2.1 and 2.2, respectively. Nonlinear static analysis was activated for the solver.

3. Results

Fig. 4 shows the load-displacement ($P-\delta$), effective crack length-displacement ($a_e-\delta$), and mode II fracture toughness-crack length (G_{II}-a_e) curves (R-curve) of the three samples tested for BL-T008 and G05B02-T008. This figure verifies the good repeatability of the test with stable crack propagation. Fig. 4(a) shows the method of defining crack initiation as the deviation of sample compliance (C) from the initial fitted linear compliance (C_0) of the sample (red line in the figure). Once sample compliance (C) becomes 5% larger than the initial defined compliance (C_0= 1/125 mm/N, in S01), the TBT method defines crack initiation. Note that due to plastic deformation in the adhesive before crack initiation, the a_e computed here using the TBT method is larger than the real crack length [27]. The displacement and load at crack initiation is different due to the slight difference in stiffness between samples.

The R-curve computed using the TBT method shows good repeatability for the three samples (Fig. 4(b)). From this figure, we can extract two main characteristics: the initiation and propagation fracture toughness, G_{IIi} and G_{IIc}, respectively. The G_{IIi} is defined at the initiation of the crack, $a_e = 40$ mm, while the G_{IIc} is defined when a fairly constant value of $G(a)$ is achieved. We computed the mean value of the three samples, which are plotted in the figure. We use this mean value in the following subsections unless specifically stated otherwise.

Fig. 4(c) and (d) shows the $P-\delta$, $a_e-\delta$, and G_{II}-a_e curves of sample G05B02-T008. Unlike the $P-\delta$ response of BL-T008, where the load increases up to a maximum value then decreases very quickly due to crack propagation, the $P-\delta$ response of G05B02-T008 shows a load increase up to local maximum value followed by a slight load decrease and then a load increase again (descending stair steps). This cycle of increased load followed by a decrease, is repeated until final failure at $\delta = 25$ mm. Moreover, this sample shows a larger maximum load and

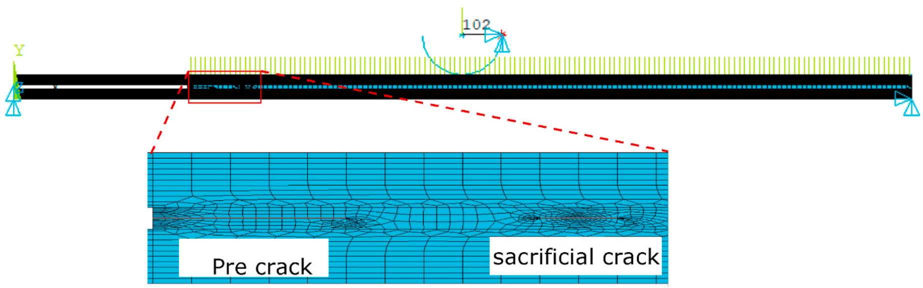

Fig. 3. FE model used for simulation elastic response of ENF test with sacrificial cracks.

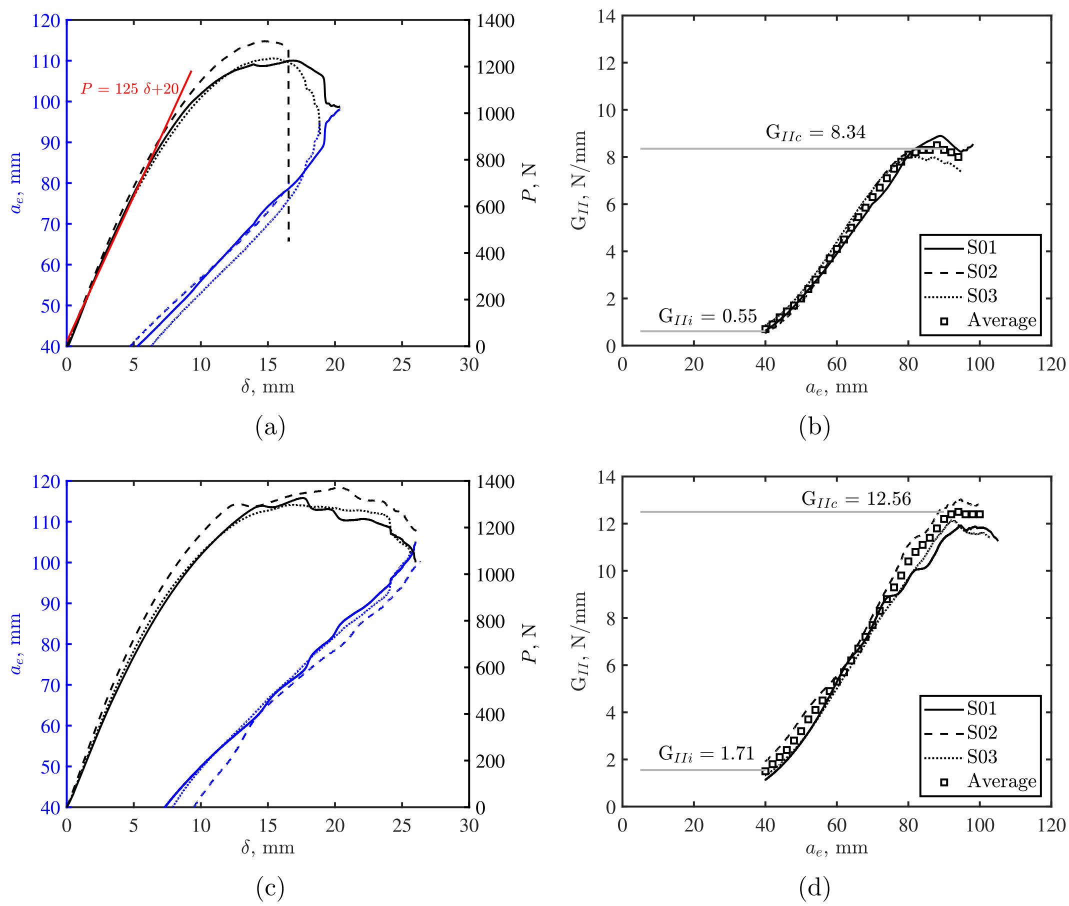

Fig. 4. ENF test response of BL-T008 and G05B02-T008: (a,c) $P-\delta$ and $a_e-\delta$ curves and (b,d) G_{II}-a_e curves, respectively. The red solid line in (a) represents the linear fitting of the elastic stiffness used to define crack initiation in the TBT method. (For interpretation of the references to color in this figure legend, the reader is referred to the Web version of this article.)

displacement and a_e at failure compared to BL-T008. The R-curve of G05B02-T008 is slightly different to BL-T008 as well, where a step-wise response is observed after $a_e \simeq 70$ mm. Additionally, G05B02-T008 shows larger G_{IIi} and G_{IIc}. These differences in the $P-\delta$ and G_{II}-a_e suggest different damage mechanisms during crack propagation.

Table 2 shows the maximum load, P_{max}, the initiation and propagation fracture toughness (G_{IIi} and G_{IIc}, respectively), and the percentage increase compared to the baseline samples for all the tested samples. A global trend is evident, whereby samples with sacrificial cracks always show larger load and fracture toughness.

4. Discussion

4.1. Toughening mechanisms

Fig. 5 shows representative $P-\delta$ and $G-a_e$ curves for the baseline sample (BL-T008) and the sample with a sacrificial crack (G05B02-T008). For the BL-T008 sample, we observe typical $P-\delta$ and $G-a_e$ curves, where the load increases until a maximum load is reached and then decreases rapidly due to the rapid propagation of the crack [10]. For the G05B02-T008 sample, the load increases up to a local maximum load (“Point a” in Fig. 5(a)), which is larger than the P_{max} for the BL-T008 sample. At this point, the crack initiates at its tip, as shown in Fig. 6(a). The existence of the sacrificial crack 5 mm from the crack tip generates two new spots for stress concentration inside the FPZ, as marked with red circles in Figs. 6(a) and Fig. 7. These new spots

Table 2
Summary of maximum load, P_{max}, initiation and propagation fracture toughness, (G_{IIi} and G_{IIc}, respectively), and the percentage of improvement (% Imp.) for all the tested samples. Samples with $g = 15$ mm failed in a catastrophic manner, and thus G_{IIc} could not be measured.

Label	P_{max}(N)	% Imp.	G_{IIi} (N/mm)	% Imp.	G_{IIc} (N/mm)	% Imp.
BL-T008	1256 ± 55	–	0.55 ± 0.19	–	8.34 ± 0.43	–
G05B02-T008	1380 ± 42	10	1.71 ± 0.25	211	12.56 ± 0.53	52
G05B05-T008	1250 ± 63	0	1.05 ± 0.31	91	9.40 ± 0.21	12
G10B02-T008	1537 ± 102	22	1.91 ± 0.54	256	10.69 ± 0.60	28
G10B05-T008	1406 ± 47	12	1.82 ± 0.19	230	9.11 ± 0.33	9
G15B02-T008	1468 ± 87	18	1.96 ± 0.28	247	–	–
G15B05-T008	1435 ± 69	14	1.83 ± 0.42	213	–	–
BL-T003	935 ± 39	–	0.52 ± 0.11	–	3.17 ± 0.55	–
G05B02-T003	1168 ± 72	25	1.02 ± 0.23	96	6.29 ± 0.37	98

redistribute stresses inside the FPZ, which reduces the stress concentration at the crack tip at the same displacement level and hence retards the crack initiation as shown in Fig. 4.

To verify the strain redistribution, we employed the FE model with and without sacrificial cracks. The displacement at which the crack initiates is defined experimentally at the crack initiation displacement determined by the TBT method (sample without sacrificial film, BL-T008) equals ≃ 6.3 mm. At this displacement, the strains at the interface reaches the critical interface strain, at which the crack grow. We applied this measured displacement to the indenter and recorded maximum von Mises strain at the crack tip at this displacement for the baseline sample. This strain is considered as the interface strain and equals 0.345. For samples with sacrificial crack (G05B02-T008), we applied the same displacement and recorded the maximum von Mises strain at the crack tip, which equaled 0.323. Therefore, to propagate a crack, more displacement had to be applied at the interface with the sacrificial film. This higher displacement achieves a larger initiation fracture toughness (see Fig. 5(b)) due to the higher deformation of the adhesive layer at the sacrificial crack.

Once the crack initiates at "Point a", the load decreases until "Point b", at which a secondary crack initiates from the sacrificial crack tip and propagates backward (in the opposite direction to the main crack propagation) at the lower interface, as shown in Fig. 6(b), which arrests the crack propagation at the upper interface. The decrease in the load between "Point a" and "Point b" corresponds to the small plateau in the R-curve at the same points (Fig. 5(b)).

Increasing the applied displacement, the load increases again while the backward secondary crack grows, forming an adhesive ligament until "Point c". Between "Point b" and "Point c", the material dissipates energy to grow the secondary crack at the lower interface and to elastically deform the adhesive ligament, which leads to increased fracture energy from 6.4 N/mm at "Point b" to 8.9 N/mm at "Point c". At this point, the stress concentration at the next sacrificial crack tip reaches the interface strength, resulting in crack growth at the upper interface, as shown in Fig. 6(d). The crack growth continues until "Point d", resulting in decreased load, at which a secondary crack grows backward at the lower interface (Fig. 6(d)).

It is notable that the maximum load, P_{max}, achieved for G05B02-T008, 1380 N, (obtained at "Point c") is larger than BL, 1256 N. Due to the propagation of a secondary crack and the compressive force that are transferred locally to the other interface, the propagation of the primary crack is governed by a mixed mode propagation, which requires larger load to propagate the crack. Therefore, to propagate the crack in the presence of secondary cracks, associated with the sacrificial cracks existence, larger load should be exerted, which increase maximum load that the joint can sustain (improved P_{max} for joints with sacrificial cracks, see Table 2).

The same scenarios between "Point b" and "Point c" and between "Point c" and "Point d" are then repeated between "Point d" and "Point e" and between "Point e" and "Point f", resulting in increased fracture energy and a plateau in the R-curve, respectively, as shown in Fig. 5(b). Note that even when the main crack reaches the indented area at $\delta = 25.9$ mm, the joint can sustain a high load due to the presence of the unbroken ligaments, as shown in Fig. 6(g). The presence of these ligaments keeps the two adherends in contact, which is not the case in the baseline joint, where a complete separation between adherends occurs, resulting in a complete loss of the joint stiffness and strength. Fig. 8 shows the 3D μ-CT micrograph and slices of G05B02-T008 after unloading the sample, reflecting the contact between the upper and lower adherends through the ligament. However, some cracks appear inside the ligament due to the large shear stresses in the adhesive ligament.

4.2. Effect of sacrificial crack topology

Fig. 9 shows that both the sacrificial crack width and the gap between the two successive cracks influence the $P - \delta$ and $G - a_e$

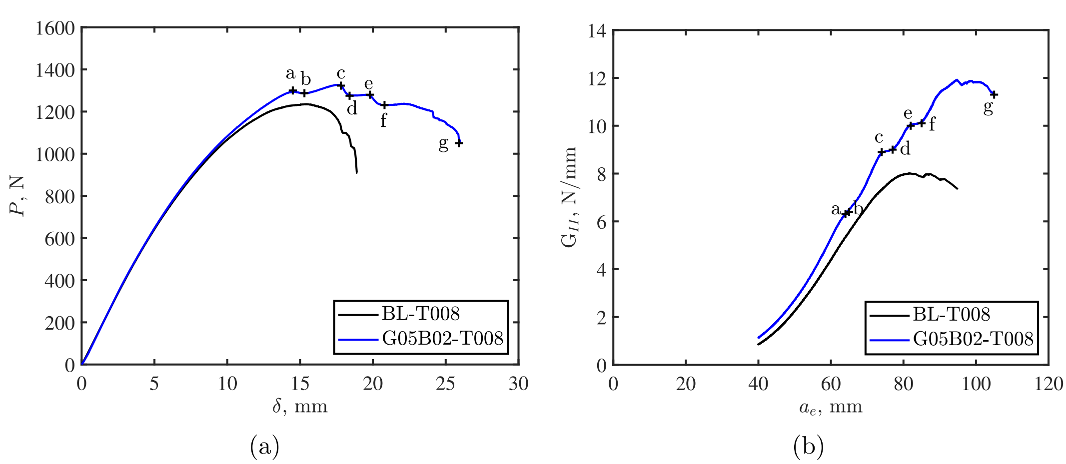

Fig. 5. Representative sample of $P - \delta$ and $G - a_e$ curves of BL-T008 and G05B02-T008 under the ENF test.

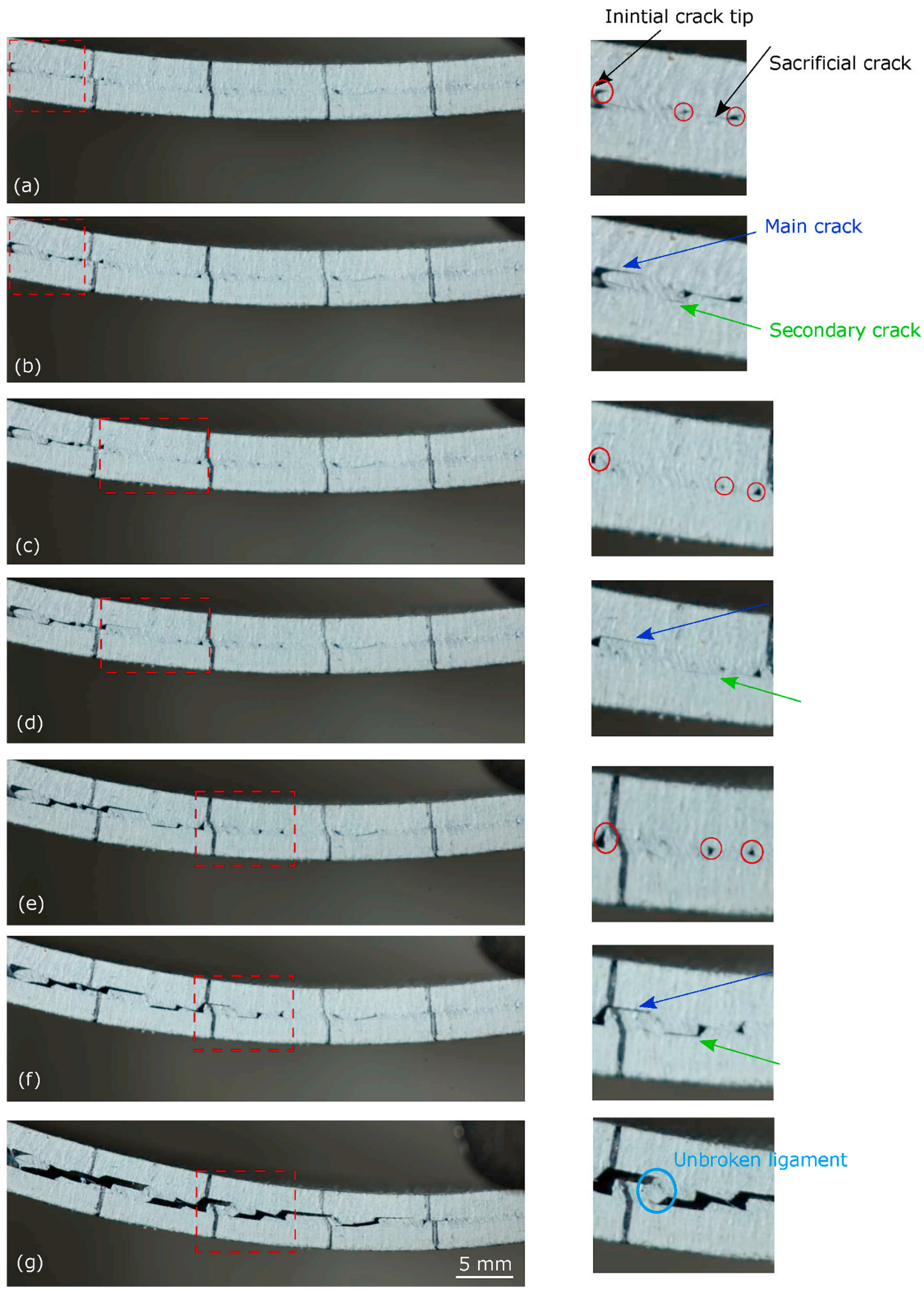

Fig. 6. Example of the sequence of crack propagation during ENF test of modified adhesive with sacrificial crack. The figures are taken for sample G05B02-S01 corresponding to points marked in Fig. 5.

responses. The solid curves and their corresponding dash curves of the same color in Fig. 9 show the effect of the gap between the two successive cracks, g, of width $B = 2$ and 5 mm, respectively. All samples with sacrificial cracks show larger P_{max}, G_{IIi} and G_{IIc}. A sacrificial crack of 2 mm width and 5 mm gap improves the P_{max}, G_{IIi} and G_{IIc} by 10%, 211% and 52%, respectively. The P_{max} improvement rate and G_{IIi} are increased to 22% and 256% for $g = 10$ mm. This improvement is due to the larger path of the secondary crack to grow at the lower interface, which allows more energy dissipation and hence higher initiation fracture toughness. Moreover, the presence of the sacrificial crack initially out of the FPZ of the initial crack allows larger deformation inside the adhesive layer, which stores higher elastic energy inside the adhesive at the tips of the sacrificial crack and hence improves P_{max} and G_{IIi}. Despite this improvement, the G_{IIc} improvement rate reduces to 28% due to the incomplete fracture process, as shown in Fig. 9(a). In this figure, we observed a decreased load at $\delta = 18.7$ mm and a slight increase at $\delta = 19.3$ mm, corresponding to “Point a” and “Point c” in Fig. 5(a) for $g = 5$ mm. However, the mechanism of the secondary crack growth and the formation of ligaments is not repeated at the next sacrificial crack due to the higher stored energy at this stage, which leads to catastrophic failure. Even with the incomplete fracture process, G_{IIc} is still larger than the baseline joints. Further increasing g to 15 mm leads to earlier failure of the joint with catastrophic failure due to the higher energy stored inside the adhesive layer as a result of the larger deformations at the sacrificial crack.

Increasing the crack width decreases P_{max}, G_{IIi} and G_{IIc} due to the reduced interfacial length that allows cracks to grow at both interfaces. For $B = 5$ mm, the interfacial length that allows for crack propagation is reduced by 3 mm at each sacrificial crack compared to $B = 2$ mm. According to linear elastic fracture mechanics, the fracture toughness is proportional to the crack length; thus, the reduced crack length in this case results in reduced fracture toughness. Again, this is true for all

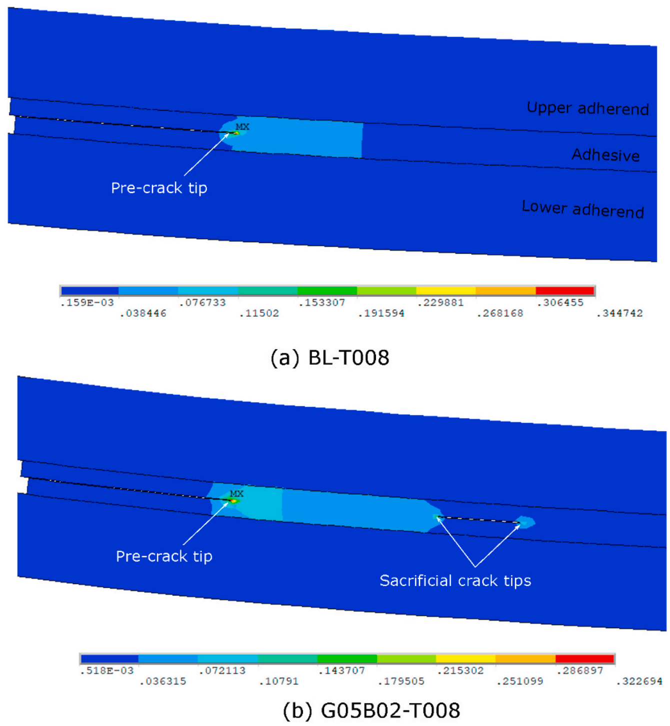

Fig. 7. Von-Misses strain maps of BL-T008 and G05B02-T008 samples.

cases; however, the percentage of improvement for $B = 5$ mm is less than that for $B = 2$ mm, the P_{max}, G_{IIi} and G_{IIc} are still larger than the baseline joint, as shown in Fig. 9(c) and (d).

4.3. Effect of adhesive thickness

Fig. 10 shows that the improvement of P_{max} and fracture toughness due to the sacrificial cracks is larger for thin adhesives. For G05B02-T003, P_{max}, G_{IIi}, and G_{IIc} are improved by 25%, 96%, and 98%, respectively, compared to BL-T003. For thin adhesive bondlines, the FPZ is small, and stresses are very concentrated at the crack tip, resulting in earlier crack growth and hence lower strength and toughness than thicker adhesive bondlines, as shown in Fig. 10 [30]. The presence of sacrificial cracks redistributes the stresses inside the adhesive layer, which increases the FPZ and hence retards the crack propagation. The FEM results for the thin adhesives are shown in 11, which provide an explanation why the sacrificial crack method is so effective for thin adhesives. In this figure, we applied displacement for baseline joint until the maximum strain reaches the critical interface strain, as determined for the thick adhesive = 0.345. The displacement that achieves this strain level equals 4.7 mm. For the sample with sacrificial crack and at the same displacement level, the maximum strain equals 0.254 (see Fig. 11), achieving 26.4% strain reduction compared to a 6.7% reduction for the thick adhesive (see Fig. 7). To achieve the critical interface strain at which cracks initiate, we increased the applied displacement to 6.05 mm, achieving 28.7% increased displacement compared to 3.6% for thick adhesives.

5. Conclusions

In this work, we present a novel technique to improve secondary bonded joints mode II fracture toughness based on creating tailored sacrificial cracks inside the adhesive layer. We demonstrated that the presence of sacrificial cracks inside the adhesive layer improves G_{IIi}, G_{IIc} and P_{max}. With 2 mm sacrificial crack length and 5 mm gap, we achieved improvements of 211%, 52% and 10% for G_{IIi}, G_{IIc} and P_{max}, respectively. The improved load capacity was due to the propagation of a secondary crack and the compressive force that are transferred locally to the other interface, which make the propagation of the primary crack is governed by a mixed mode propagation and hence requires larger load to propagate the crack. The improved fracture toughness was due to the growth of a secondary crack at the lower interface, which arrested growth of the crack at the upper interface and formed adhesive ligament. Moreover, the dissipation of more energy due to deformation of the created ligaments contributed to higher fracture energy. Increasing the gap to 10 mm improved P_{max} and G_{IIi} due to the increase of the allowed interfacial length for the secondary crack to propagate at the lower interface. However, once the first sacrificial crack was passed, catastrophic failure occurred due to the excess stored energy in the system, resulting in a reduced improvement in G_{IIc}. Increasing the sacrificial crack width reduced the fracture toughness due to the

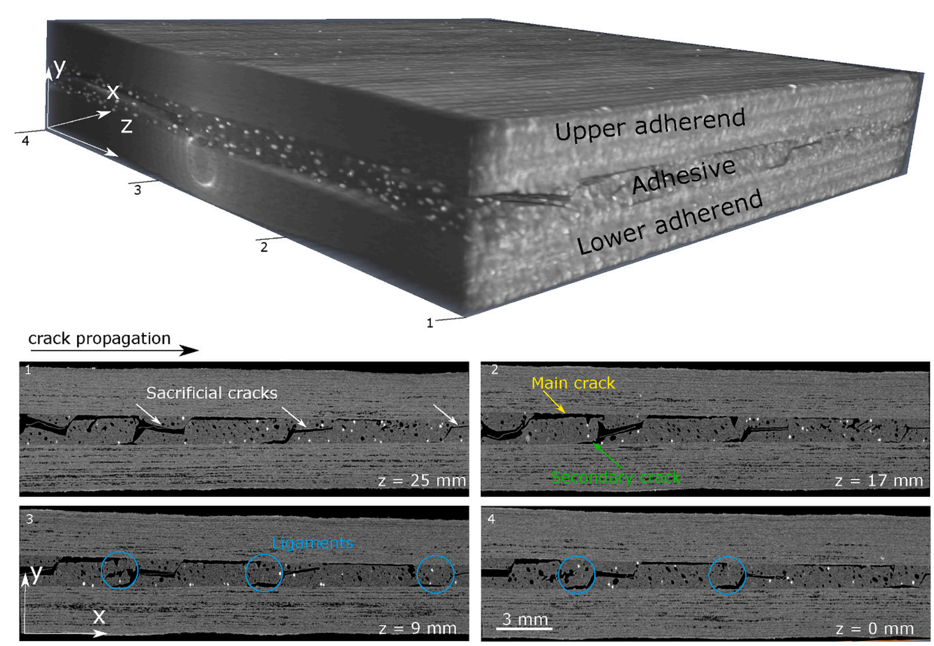

Fig. 8. 3D μ-CT micrographs of G05B02-T008 sample and 2D micrographs through the sample width.

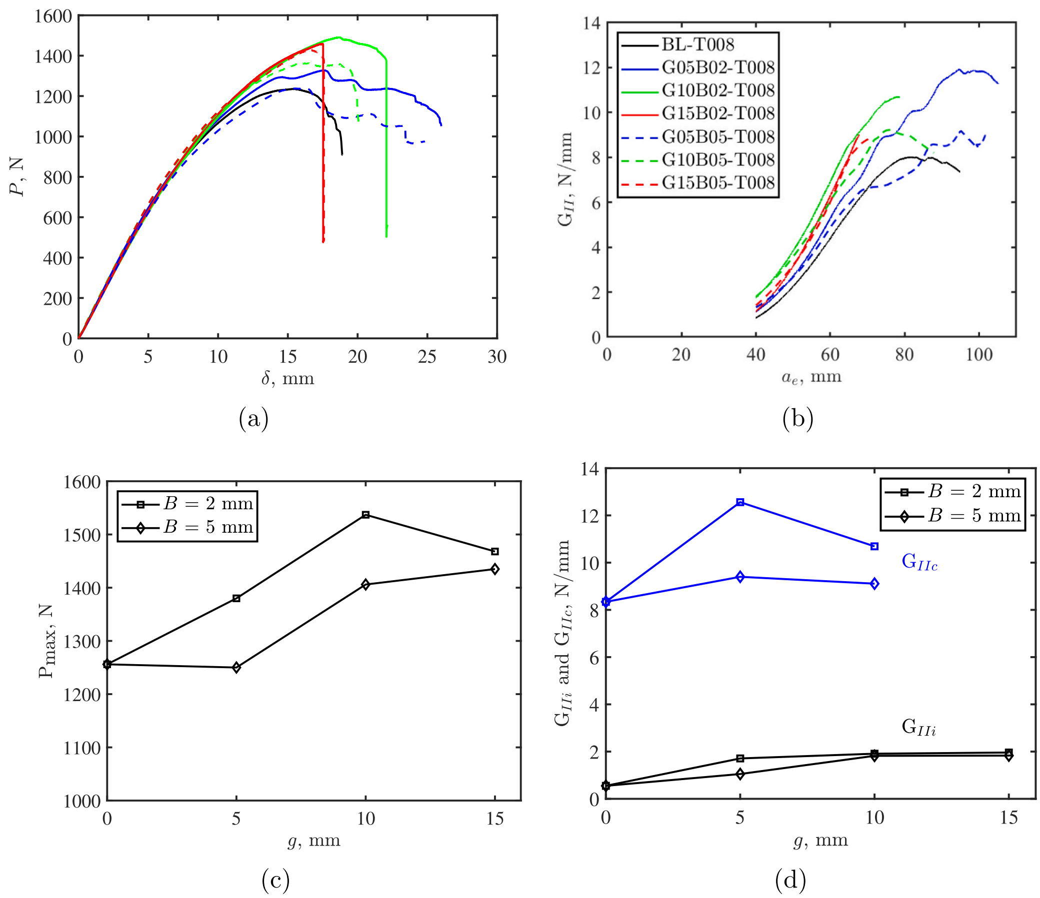

Fig. 9. Effect of sacrificial crack width and the gap between two successive cracks on ENF test response: (a) $P-\delta$, (b) $G-a_e$ and (c and d) summary of P_{max}, G_{IIi} and G_{IIc} with respect to B and g.

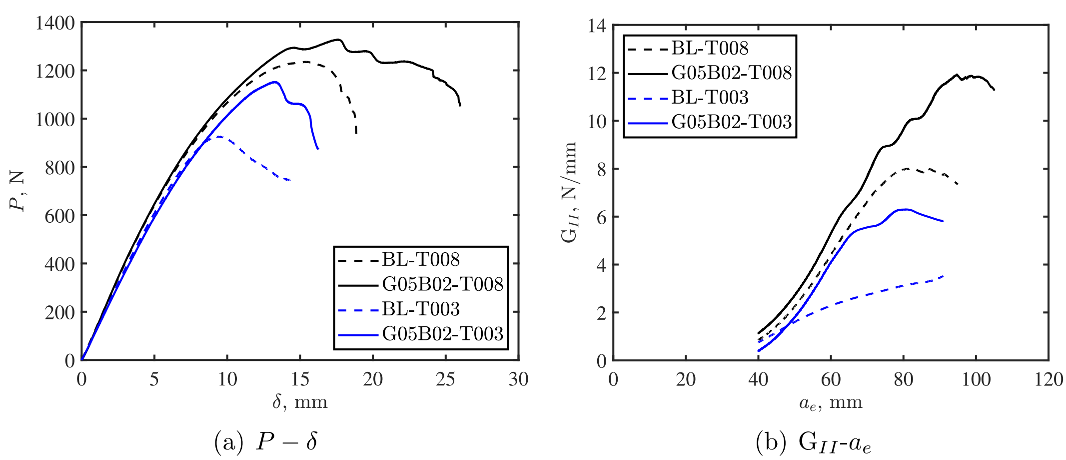

Fig. 10. Effect of adhesive thickness on ENF response of baseline samples and samples with sacrificial cracks.

reduction of the interfacial length that allowed crack propagation to occur at the lower interface. Our technique was more effective for thin adhesive bondlines than for thick adhesives due to the larger increase of the FPZ in the thin adhesives with embedding sacrificial cracks.

From applicability point of view, the proposed method can be automated in manufacturing real structures by adding the PTFE film with previously generated cutouts over the adhesive layer prior to bonding. Moreover, for thermoplastic adhesive the PTFE film can be sued as a carrier for adhesive layer and built the adhesive tape over the PTFE film with required sacrificial crack width and gap. In view of our results that proved the improved Mode II toughness by embedding sacrificial cracks inside the bondline, and based on the fact that the crack initiation in single and double lab joints is governed by mode I, while crack propagation is governed by Mode II crack propagation due to shear stresses [31,32], we expect toughness improvement of the single and double lab joints. However, we recommend to extend this study to evaluate the effectiveness of embedding sacrificial cracks inside adhesive joints under mode I and mixed mode propagation. Additionally, it is advised to apply the proposed method for structural joint such as: single- and double-lap and T-joints to evaluate the efficiency of this method in

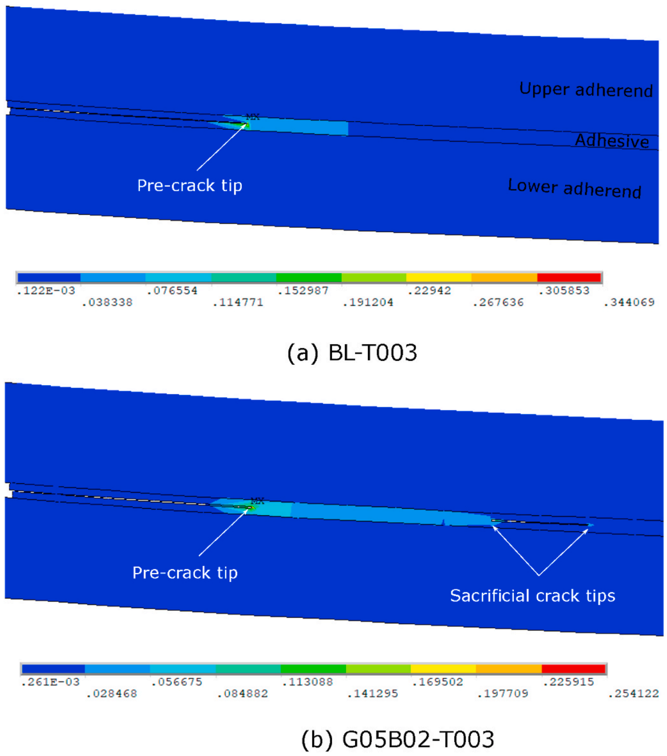

Fig. 11. Von-Misses strain maps of BL-T003 and G05B02-T003 samples.

real application structures.

Author contributions

A.W. and G.L. conceptualized the study. A.W. performed the experiments and analyzed the data.

All authors contributed to writing and editing the manuscript.

Declaration of competing interest

The authors declare that they have no known competing financial interests or personal relationships that could have appeared to influence the work reported in this paper.

Acknowledgement

This research was funded by King Abdullah University of Science and Technology Office of Sponsored Research (OSR) under award number OSR-2017-CRG6-3388.01.

References

[1] J.D. Russell, Composites affordability initiative: transitioning advanced aerospace technologies through cost and risk reduction, AMMTIAC Q. 1 (3) (2006) 3–6.
[2] F. Matthews, P. Kilty, E. Godwin, A review of the strength of joints in fibre-reinforced plastics. part 2. adhesively bonded joints, Composites 13 (1) (1982) 29–37.
[3] S. Prolongo, M. Gude, G. Del Rosario, A. Ureña, Surface pretreatments for composite joints: study of surface profile by SEM image analysis, J. Adhes. Sci. Technol. 24 (11–12) (2010) 1855–1867.
[4] J. Holtmannspötter, J. Czarnecki, M. Wetzel, D. Dolderer, C. Eisenschink, The use of peel ply as a method to create reproduceable but contaminated surfaces for structural adhesive bonding of carbon fiber reinforced plastics, J. Adhes. 89 (2) (2013) 96–110.
[5] F. Boerio, B. Roby, R. Dillingham, R. Bossi, R. Crane, Effect of grit-blasting on the surface energy of graphite/epoxy composites, J. Adhes. 82 (1) (2006) 19–37.
[6] R. Dillingham, B. Oakley, Surface energy and adhesion in composite–composite adhesive bonds, J. Adhes. 82 (4) (2006) 407–426.
[7] R. Moreira, V. Oliveira, F. Silva, R. Vilar, M. de Moura, Mode II fracture toughness of carbon–epoxy bonded joints with femtosecond laser treated surfaces, Int. J. Mech. Sci. 148 (2018) 707–713.
[8] V. Oliveira, S. Sharma, M. De Moura, R. Moreira, R. Vilar, Surface treatment of cfrp composites using femtosecond laser radiation, Optic Laser. Eng. 94 (2017) 37–43.
[9] R. Tao, M. Alfano, G. Lubineau, In situ analysis of interfacial damage in adhesively bonded composite joints subjected to various surface pretreatments, Compos. Appl. Sci. Manuf. 116 (2019) 216–223.
[10] A. Wagih, R. Tao, A. Yudhanto, G. Lubineau, Improving mode ii fracture toughness of secondary bonded joints using laser patterning of adherends, Compos. Part A 134 (2020) 1–11.
[11] R. Tao, X. Li, A. Yudhanto, M. Alfano, G. Lubineau, On controlling interfacial heterogeneity to trigger bridging in secondary bonded composite joints: an efficient strategy to introduce crack-arrest features, Compos. Sci. Technol. 188 (2020) 107964.
[12] R. Tao, M. Alfano, G. Lubineau, Laser-based surface patterning of composite plates for improved secondary adhesive bonding, Compos. Appl. Sci. Manuf. 109 (2018) 84–94.
[13] P. Chang, A. Mouritz, B. Cox, Properties and failure mechanisms of pinned composite lap joints in monotonic and cyclic tension, Compos. Sci. Technol. 66 (13) (2006) 2163–2176.
[14] A.B. Nair, P. Sivasubramanian, P. Balakrishnan, K.A.N.A. Kumar, M.S. Sreekala, in: Sabu Thomas, Kuruvilla Joseph, S.K. Malhotra (Eds.), Environmental Effects, Biodegradation, and Life Cycle Analysis of Fully Biodegradable Green Composites, 2014.
[15] L.K. Jain, K.A. Dransfield, Y.W. Mai, On the effects of stitching in CFRPs-II. Mode II delamination toughness, Compos. Sci. Technol. 58 (6) (1998) 829–837.
[16] A. Yudhanto, G. Lubineau, I.A. Ventura, N. Watanabe, Y. Iwahori, H. Hoshi, Damage characteristics in 3d stitched composites with various stitch parameters under in-plane tension, Compos. Appl. Sci. Manuf. 71 (2015) 17–31.
[17] J. Kim, C. Baillie, J. Poh, Y.W. Mai, Fracture toughness of CFRP with modified epoxy resin matrices, Compos. Sci. Technol. 43 (3) (1992) 283–297.
[18] L.C. Tang, H. Zhang, S. Sprenger, L. Ye, Z. Zhang, Fracture mechanisms of epoxy-based ternary composites filled with rigid-soft particles, Compos. Sci. Technol. 72 (5) (2012) 558–565.
[19] T. Löbel, D. Holzhüter, M. Sinapius, C. Hühne, A hybrid bondline concept for bonded composite joints, Int. J. Adhesion Adhes. 68 (2016) 229–238.
[20] S. Heide-Jørgensen, S.T. de Freitas, M.K. Budzik, On the fracture behaviour of CFRP bonded joints under mode I loading: effect of supporting carrier and interface contamination, Compos. Sci. Technol. 160 (2018) 97–110.
[21] A. Yudhanto, M. Almulhim, R. Tao, L. Fatta, M. Alfano, G. Lubineau, Enhancement of fracture toughness in secondary bonded cfrp using hybrid thermoplastic/thermoset bondline architecture, Compos. Sci. Technol. 199 (2020) 108346–108352.
[22] A. Chudnovsky, S. Wu, Effect of crack-microcracks interaction on energy release rates, Int. J. Fract. 44 (1) (1990) 43–56.
[23] G. Bullegas, S.T. Pinho, S. Pimenta, Engineering the translaminar fracture behaviour of thin-ply composites, Compos. Sci. Technol. 131 (2016) 110–122.
[24] K. Maloney, N. Fleck, Toughening strategies in adhesive joints, Int. J. Solid Struct. 158 (2019) 66–75.
[25] L.A. Carlsson, J.W. Gillespie, B.R. Trethewey, Mode II interlaminar fracture of graphite/epoxy and graphite/PEEK, J. Reinforc. Plast. Compos. 5 (3) (1986) 170–187, https://doi.org/10.1177/073168448600500302.
[26] S. Hashemi, A.J. Kinloch, J. Williams, The analysis of interlaminar fracture in uniaxial fibre-polymer composites, Proc. R. Soc. London A Math. Phys. Sci. 427 (1872) (1990) 173–199.
[27] M. Budzik, J. Jumel, N.B. Salem, M. Shanahan, Instrumented end notched flexure–crack propagation and process zone monitoring Part II: data reduction and experimental, Int. J. Solid Struct. 50 (2) (2013) 310–319.
[28] M. Pérez-Galmés, J. Renart, C. Sarrado, A. Brunner, A. Rodríguez-Bellido, Towards a consensus on mode II adhesive fracture testing: experimental study, Theor. Appl. Fract. Mech. 98 (2018) 210–219.
[29] R. Fernandes, J. Chousal, M. De Moura, J. Xavier, Determination of cohesive laws of composite bonded joints under mode II loading, Compos. B Eng. 52 (2013) 269–274.
[30] L.F. da Silva, F. De Magalhaes, F. Chaves, M. De Moura, Mode II fracture toughness of a brittle and a ductile adhesive as a function of the adhesive thickness, J. Adhes. 86 (9) (2010) 891–905.
[31] S. Oshima, A. Yoshimura, S. Yashiro, Y. Hirano, T. Ogasawara, Experimental and analytical validation of mode ii fracture toughness tests for a type of double-lap joint, Compos. Struct. 234 (2020) 111757–111763.
[32] S. Panigrahi, B. Pradhan, Onset and growth of adhesion failure and delamination induced damages in double lap joint of laminated frp composites, Compos. Struct. 85 (4) (2008) 326–336.